Frequency domain fluorescence optical imaging using a finite element method

Yaling Pei*, Yuqi Yao* [1], Feng-Bao Lin*, and Randall L. Barbour‡

* Polytechnic University, Brooklyn, NY 11201

‡ SUNY Health Science Center, Brooklyn, NY 11203

ABSTRACT

In this paper, a reconstruction algorithm for fluorescence yield and lifetime imaging in dense scattering media is formulated and implemented. Two frequency domain radiation transport equations based on the diffusion approximation are used to model the migration of excitation and emitted photons. In the forward formulation, a finite element approach, which is specially effective for complex geometries and inhomogeneous distribution of medium properties, is adopted to obtain the required imaging operator and the simulated detector responses related to the photon fluxes on the boundary. Inverse formulation is derived based on the integral form of two diffusion equations. The technique is demonstrated by reconstructing spatial images of heterogeneous fluorophore distribution and lifetime using simulated data obtained from homogeneous and complex (*i.e.*, MRI breast map) media containing objects with fluorophore and with and without added noise.

Keywords: fluorescence optical imaging, image reconstruction, inverse scattering, diffusion approximation, finite element method, CGD method

1. INTRODUCTION

Over the past several years, fluorescence studies of tissue have been explored as a potential tool to provide useful diagnostic information [1, 2]. Recently, these have been extended to include model studies of thick tissues [3-7] which have provided insight into the possibility of acquiring spatial maps of important physiological states and metabolite levels (*e.g.*, tissue oxygenation, pH, Ca^{++}, lipid environments, *etc.*,) derived from analysis of tomographic data sets. These include reports by Chang *et al.* [8], O'Leary *et al.* [9] and Paithankar and Sevick-Muraca [10], who have described formulations that yield spatial maps of fluorescence yield and fluorophore lifetime based on inverse computations derived from data obtained from solution to the diffusion [9,10] and transport [8] equation.

In this paper, we extend recent computation and experimental studies [8, 11] by our group and describe results obtained that simultaneously compute images of fluorescence yield and fluorophore lifetime. These studies consider a bounded medium having either a uniform background or an anatomically accurate background of the female breast derived from MRI data. Included in these backgrounds are one or two inclusions, simulating a pathology (*e.g.*, tumor), that differs in their absorption and scattering contrast with the background and in the amount of fluorophore present. Also modeled are examples in which a varying amount of fluorophore was present in the background. Solutions to the forward problem were obtained using the finite element method. Inverse formulations were derived from a scattering integral equation which describe the perturbation produced by the added fluorophore using the technique described in [12]. Image reconstructions are performed using a regularized least squares approach based on conjugate gradient descent (CGD) algorithm [13]. The results obtained demonstrate the ability to reconstruct images of fluorescence yield and fluorophore lifetime in media having homogeneous and complex backgrounds.

2. THE MATHEMATICAL FORMULATION

It is known that propagation of photons through a dense scattering medium with low absorption can be accurately described by the diffusion approximation to the radiation transport equation. Consider one or more objects (scatterers) with fluorophore embedded in a inhomogeneous scattering background medium occupying a domain Ω with

[1] He is now with Bell Labs, Lucent Technologies.

SPIE Vol. 2979 • 0277-786X/97/$10.00

boundary Ω_s, such as human tissue. In the frequency-domain, the excitation field, $u^x(\mathbf{r}', r_s)$, at any location r' due to an amplitude-modulated point source at location r_s, and the subsequently produced emission field of fluorescent photons, $u^m(\mathbf{r}, r')$, at any detector position r can be represented by a coupled diffusion equation as:

$$\nabla \cdot [D^x(\mathbf{r}')\nabla u^x(\mathbf{r}', \mathbf{r}_s)] + [-\mu_a^x(\mathbf{r}') - \mu_f(\mathbf{r}') + i\frac{\omega}{v}]u^x(\mathbf{r}', \mathbf{r}_s) = -\delta(\mathbf{r}' - \mathbf{r}_s), \tag{1}$$

and

$$\nabla \cdot [D^m(\mathbf{r})\nabla u^m(\mathbf{r}, \mathbf{r}')] + [-\mu_a^m(\mathbf{r}) + i\frac{\omega}{v}]u^m(\mathbf{r}, \mathbf{r}') = -S^m(\mathbf{r}'), \tag{2}$$

where superscripts x and m represent the excitation light and emission light, respectively, $D^x = 1/3(\mu_a^x + \mu_f + \mu_s'^x)$ the optical diffusion coefficient for excitation light, $D^m = 1/3(\mu_a^m + \mu_s'^m)$ is the diffusion coefficient for emission light, μ_a and μ_s' are the absorption coefficient and the reduced scattering coefficient, μ_f the fluorophore absorption coefficient associated with the local concentration of fluorescent probes, ω the modulation frequency, v the speed of light, and S^m the emission source, which is given by

$$S^m(\mathbf{r}') = \frac{\eta}{(1 - j\omega\tau)}u^x(\mathbf{r}'). \tag{3}$$

Here, η is called fluorescence yield, which is the product of fluorophore absorption coefficient, μ_f, and fluorescent quantum yield, γ, $(i.e., \eta = \mu_f\gamma)$. $\gamma = \tau/\tau_0$. τ_0 is the intrinsic lifetime of the fluorophore, and τ the fluorophore lifetime.

The photon fluxes on Ω_s corresponding to the excitation light and the emission light can be determined from Fick's law:

$$J^x(\mathbf{r}) = -D^x(\mathbf{r})\hat{\mathbf{n}} \cdot \nabla u^x(\mathbf{r})|_{\Omega_s}, \tag{4}$$

and

$$J^m(\mathbf{r}) = -D^m(\mathbf{r})\hat{\mathbf{n}} \cdot \nabla u^m(\mathbf{r})|_{\Omega_s}, \tag{5}$$

where $\hat{\mathbf{n}}(\mathbf{r})$ is the normal unit vector of Ω_s.

In this paper, we employ the finite element method to solve Eqs. (1) and (2) with the zero fluence boundary conditions, $(i.e., u^x = 0$ on Ω_s and $u^m = 0$ on $\Omega_s)$, to obtain the solution of the forward problem. For solution of the inverse problem, two step reconstructions are required in the general case where no previous knowledge about the optical properties of the medium are known. The first solution is solved for the absorption and diffusion coefficients of the medium, and the second uses this result to compute the expected excitation field from which we derive the imaging operator followed by the fluorescence yield and fluorophore lifetime. Here we employ an inverse formulation to compute $\delta\eta$ and $\delta\tau$ based on a scattering integral equation similar to that previously described in [12] assuming μ_a and D known.

By considering the actual medium as perturbation from a background, we define the position-dependent incremental changes in the fluorophore optical properties with respect to the background to be:

$$\delta\eta(\mathbf{r}) = \eta(\mathbf{r}) - \eta_b(\mathbf{r}), \quad \text{and} \quad \delta\tau(\mathbf{r}) = \tau(\mathbf{r}) - \tau_b(\mathbf{r}), \tag{6}$$

where the corresponding changes of the fluorescent photon density and the fluorescent photon flux are denoted as

$$\delta u^m(\mathbf{r}) = u^m(\mathbf{r}) - u_b^m(\mathbf{r}) \tag{7}$$

and

$$\delta J^m(\mathbf{r}) = J^m(\mathbf{r}) - J_b^m(\mathbf{r}). \tag{8}$$

By inserting Eq. (7) into Eq. (2) in such a way as to isolate the source term S^m corresponding to the background in the right-hand side, we have

$$\nabla \cdot [D^m(\mathbf{r})\nabla u^m(\mathbf{r}, \mathbf{r}') + [-\mu_a^m(\mathbf{r}) + i\frac{\omega}{v}]u^m(\mathbf{r}, \mathbf{r}') = -S_b^m(\mathbf{r}') - f_s^m(\mathbf{r}'), \tag{9}$$

where

$$S_b^m(\mathbf{r}') = \frac{\eta_b}{1 - j\omega\tau_b}u^x(\mathbf{r}') \tag{10}$$

and

$$f_s^m(\mathbf{r}') = O(\mathbf{r}')u^x(\mathbf{r}'), \tag{11}$$

where O is a complex function of fluorescence yield, η, and fluorophore lifetime, τ, and

$$O(\eta(\mathbf{r}'), \tau(\mathbf{r}')) = \frac{\eta(\mathbf{r}')}{1 - j\omega\tau(\mathbf{r}')} - \frac{\eta_b(\mathbf{r}')}{1 - j\omega\tau_b(\mathbf{r}')}. \tag{12}$$

The volume integral equation for the perturbation of fluorescent photon density can be expressed by

$$\delta u^m(\mathbf{r}) = \int_\Omega O(\mathbf{r}')u^x(\mathbf{r}')G^m(\mathbf{r}, \mathbf{r}')d\mathbf{r}', \tag{13}$$

while the perturbation of fluorescent photon flux on the surface of the bounded medium can be given by

$$\delta J^m(\mathbf{r}) = -D^m(\mathbf{r})\hat{\mathbf{n}} \cdot \nabla \delta u^m(\mathbf{r}). \tag{14}$$

Using the finite element technique, let N and M denote the total number of the nodes and elements, respectively, L the number of the nodes on the boundary, d the number of detectors for each source, s the number of sources, and Ω_j the region of the j^{th} element.

The perturbation of fluorescent output flux vector $\delta\mathbf{J}^{m(p)}$ at detector location $(\xi_1, \xi_2, \cdots, \xi_d)$ for p^{th} source configuration can be expressed as

$$\delta\mathbf{J}^{m(p)} = \mathbf{T}\ \delta\mathbf{u}^{m(p)}, \tag{15}$$

where, T is a $d \times (N - L)$ transformation matrix, which can be computed from Eq. (3) using the FEM technique, and $[\delta\mathbf{u}^{m(p)}]^T = [\delta u_1^{m(p)}\ \delta u_2^{m(p)} \cdots \delta u_k^{m(p)} \cdots \delta u_{N-L}^{m(p)}]$ is the interior nodal field perturbation vector due to perturbations $\delta\eta$ and $\delta\tau$, in which

$$\delta u_k^{m(p)} = \sum_{j=1}^{M} O_j \int_{\Omega_j} u^{x(p)}(\mathbf{r}')G^m(\mathbf{r}_k, \mathbf{r}')d\mathbf{r}'. \tag{16}$$

Note that $\delta u_k^{(p)}$ is the perturbation of the fluorescent photon density at the k^{th} interior node due to the p^{th} source. We can rewrite $\delta\mathbf{u}^{m(p)}$ in a matrix notation:

$$\delta\mathbf{u}^{m(p)} = \mathbf{B}^{(p)}\mathbf{O}, \tag{17}$$

where $\mathbf{O}^\mathbf{T} = [O_1\ O_2\ \cdots\ O_M]$. The entries of $\mathbf{B}^{(p)}$ are computed from

$$B_{kj}^{(p)} = \int_{\Omega_j} u^{x(p)}(\mathbf{r}')G^m(\mathbf{r}_k, \mathbf{r}')d\mathbf{r}'. \tag{18}$$

Substituting Eq. (18) into Eq. (16), $\delta\mathbf{J}^{m(p)}$ can be represented as

$$\delta\mathbf{J}^{m(p)} = \mathbf{T}\ \mathbf{B}^{(p)}\mathbf{O} = \mathbf{W}^{(p)}\mathbf{O}, \tag{19}$$

where

$$\mathbf{W}^{(p)} = \mathbf{T}\ \mathbf{B}^{(p)}. \tag{20}$$

A complete perturbation equation can be obtained by Eq. (15) for all sources as:

$$\delta\mathbf{J}^m = \mathbf{W}\mathbf{O}, \tag{21}$$

where

$$\mathbf{W} = \begin{bmatrix} \mathbf{W}^{(1)} \\ \cdot \\ \cdot \\ \cdot \\ \mathbf{W}^{(s)} \end{bmatrix}, \quad \delta\mathbf{J} = \begin{bmatrix} \delta\mathbf{J}^{m(1)} \\ \cdot \\ \cdot \\ \cdot \\ \delta\mathbf{J}^{m(s)} \end{bmatrix}. \tag{22}$$

In fact, only those $\delta u_k^{(p)}$ connected to detector locations contribute to $\delta \mathbf{J}^{(p)}$. Therefore, for a complete weight matrix $\mathbf{W}$, only $s + \alpha \times d$ FEM runs are required, where α is the number of nodes connecting with each detector location which can vary with the type of element and generated mesh used in FEM. For 2-D cases using linear triangular elements, α is usually a value equal to or less than 3.

Object function O can be solved from Eq. (21), from which $\delta\eta$ and $\delta\tau$ can be derived from the real and imaginary parts of the object function O. So, we have from Eq. (12):

$$Re(O) = \frac{\eta_b + \delta\eta}{1 + \omega^2(\tau_b + \delta\tau)^2} - \frac{\eta_b}{1 + \omega^2\tau_b^2} \tag{23}$$

and

$$Im(O) = \omega \left[\frac{(\eta_b + \delta\eta)(\tau_b + \delta\tau)}{1 + \omega^2(\tau_b + \delta\tau)^2} - \frac{\eta_b\tau_b}{1 + \omega^2\tau_b^2} \right]. \tag{24}$$

Solving the above two equations, $\delta\eta$ and $\delta\tau$ can be obtained as follows:

$$\delta\tau = \frac{\frac{\eta_b\tau_b}{1 + \omega^2\tau_b^2} + \frac{Im(O)}{\omega}}{\frac{\eta_b}{1 + \omega^2\tau_b^2} + Re(O)} - \tau_b \tag{25}$$

and

$$\delta\eta = \left[\frac{\eta_b}{1 + \omega^2\tau_b^2} + Re(O) \right] \left[1 + \omega^2(\tau_b + \delta\tau)^2 \right] - \eta_b. \tag{26}$$

The expression given in Eqs. (25) and (26) consider the general case where fluorophore is present in the background. For most practical applications of clinical interest, this level might well be small and can be safely ignored as previously considered [9]. In situations where it is not, estimates can be made in which case iterative procedures should be adopted.

3. SIMULATION RESULTS

In this section, we show some results to demonstrate a working implementation of the reconstruction algorithm described above. We provide examples of representative results obtained from two different bounded media, one homogeneous and other complex, the latter being represented by a MRI map of the breast. Five different test cases were explored. Case I-IV are all based on an otherwise homogeneous background having cylindrical geometry to which fluorophore was added to an included object and/or to the background medium. Case V considers as similar situation except the background is represented by a 2-D MRI image of an adult female breast segmented into fat and parenchyma tissue. Added to this are two inclusions whose absorption, scattering and fluorescent properties differ from each other and from the background tissue. All computations made are 2-D for both forward and inverse calculations. The latter were computed in the presence and absence of up to 3% added noise and limited to the first Born approximation.

3.1 Fluorescence Imaging in Simple Media

In our implementation we used the Dirichlet boundary condition u = 0 on the physical boundary, and 10 point sources evenly spaced at a position $d \approx 1/\mu_s'$ below the physical boundary. For each source position photon flux values corresponding to a total of ten detectors, uniformly spaced on the physical boundary, were obtained yielding a total of 100 source-detector measurements. The medium has a radius of 4 cm and was divided into 1800 elements. The source modulation frequency is 50 MHz. the intrinsic life time, τ_0, of the added fluorophore was 10 nsec. Table 1 lists the optical properties of the added inclusions and background media for the different test cases examined.

Case I: Here we considered a homogeneous medium having a total optical thickness of approximately 40 transport mean free pathlengths. Added to this was a single diamond shaped inclusion having a diagonal dimension of approximately 1.3 cm, and absorption and reduced scattering values are double those of the background. Added fluorophore was restricted to the inclusion. Reconstruction results are shown in Figure 2.

Table 1: **Optical Properties Assigned to the Test Cases**

Test Cases		Background Medium				Target Medium 1				Target Medium 2			
		μ_a (cm^{-1})	μ_s' (cm^{-1})	μ_f (cm^{-1})	τ (ns)	μ_a (cm^{-1})	μ_s' (cm^{-1})	μ_f (cm^{-1})	τ (ns)	μ_a (cm^{-1})	μ_s' (cm^{-1})	μ_f (cm^{-1})	τ (ns)
Case I		0.02	5	–	–	0.04	10	0.004	1	–	–	–	–
Case II		0.02	5	0.001	0.5	0.04	10	0.004	1	–	–	–	–
Case V	F*	0.04	10	0.0005	0.5	0.07	6.0	0.001	1	0.06	9.0	0.0015	2
	P**	0.08	7.0										

* F represents Fat.

** P represents Parenchyma.

Case II: This test is identical to case I, except with additional fluorophore being present in the background. For this example it was assumed that the properties of the fluorophore present in the background were known, *a priori*, and thus the perturbation was limited to added fluorophore in the inclusion. Reconstruction results are shown in Figure 3.

Case III: this test is identical to case II except no prior knowledge regarding the background fluorophore properties are assumed. Here the perturbation is due to the fluorophore being present in different amounts in both the background and inclusion. Reconstruction results are shown in Figure 4.

Case IV: This test serves to determine the ability to recover the properties of fluorophore uniformly distributed in a uniform medium. The background optical properties are the same as in case I except no inclusion is present, rather added fluorophore is distributed uniformly. Reconstruction results are shown in Figure 5.

3.2 Fluorescence Imaging in Complex Media

To model light propagation in tissue, we acquire a MRI image of the breast from an adult volunteer as described previously [14]. A transverse section [7] located approximately half-way between the chest wall and nipple, shown in Figure 1, was reconstructed from 24 sagittal images and segmented according to fat (darker regions) and parenchyma (lighter regions) tissues. Added to this, symmetrically displaced from the center, were two diamond shaped inclusions having a diagonal length of approximately 0.9 cm. Optical properties of the target and those of the background tissue are listed in Table 1. To simplify computation of the flux associated with an irregular boundary, we extended the boundary of the breast to conform to circular geometry having a radius of 4 cm. The properties of the extended regions were arbitrarily designated to correspond to fat tissue. The measurement geometry used here was the same as that employed with the simple phantom above. The total optical thickness of the breast phantom is approximately 80 transport mean free path lengths.

Case V: This test explored our ability to spatially resolve two added inclusions having different fluorescence yield and fluorophore lifetime values in the presence of fluorophore in the background tissue whose properties were known *a priori*. Results shown in Figure 6 are for the case where contrast between inclusions and background media is low. Not shown are test cases where higher contrast between inclusion and background is present and similar results were obtained.

4. SUMMARY AND DISCCUSION

In this paper, we present a reconstruction algorithm for fluorescence yield and lifetime imaging in a bounded dense scattering media based on diffusion model of propagation of fluorescent photons. A finite element approach is adopted in solving the forward problem to compute the simulated detector responses associated with the photon fluxes on the boundary and to obtain the required imaging operator. The inverse formulation is derived based on a scattering integral equation which describes the perturbation produced by the added fluorophore. Image reconstructions are

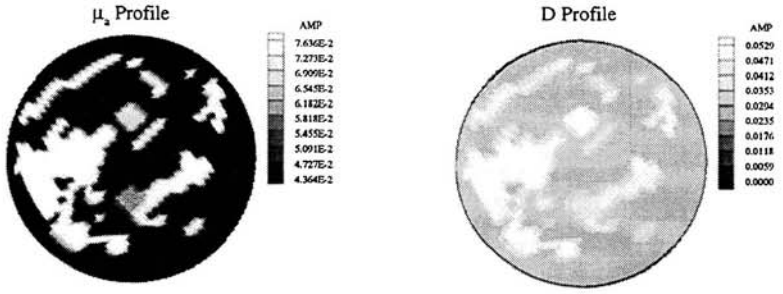

(a) (b)

Figure 1: The distribution of the absorption (a) and diffusion (b) coefficients in an axial slice derived from the MRI data. Two "pathologies" are added to the background medium.

performed using a regularized least squares approach based on CGD algorithm. The results obtained show that for a single target (cases I, II and III) in a homogeneous background, the target position can be accurately located with computed lifetime values being more accurate than fluorescence yield values even up to 3% noise is added. Qualitatively similar results are obtained in the case of two targets located in heterogeneous background media (*i.e.*, MRI data), but with greater sensitivity to added noise. We have also shown that recovery of accurate target position is possible in the presence of background fluorophore with 3% added noise.

Results shown in Figure 5 have added significance. Here we have examined the ability to recover fluorophore properties when the perturbation is uniformly distributed throughout the medium. Results obtained demonstrate a large artifact in the vicinity of the sources even in the absence of added noise. We believe this result can be traced primarily to the boundary conditions employed. Here, selection of Dirichlet boundary conditions was made in part for convenience and partially from the expectation that knowledge of exact boundary conditions in any physical measurement on an unknown medium, will never be known with certainty. The assertion of zero intensity at the boundary is clearly not physically accurate, especially near the source. Despite this, inspection of results for cases I-III show predominately artifact free results in the absence of added noise and acceptable solutions even in the presence of 3% noise for cases I and II. Case III, which has perturbation throughout the medium, produces a qualitatively correct solution in the presence of 3% noise, but has enhanced artifact near the boundary. Comparison of these finding, together with results from Figure 5 indicate that the error introduced by Dirichlet boundary conditions is nonlinear, having its maximal effect near the physical boundary. In spite of this, we find it encouraging that for a centrally buried target, the most difficult region to detect, it is possible to recover target location with good precision and obtain quantitatively accurate results for fluorophore life time.

In summary, the present studies serve to confirm and extend original reports from our group [8,11] based on laboratory experiments that qualitatively accurate images of fluorescent objects buried in dense scattering media can be recovered from tomographic measurements.

ACKNOWLEDGEMENTS

This work was supported in part by the National Institutes of Health under Grant # R01-CA59955, R01-CA66184, and ONR grant # N000149510063.

REFERENCES

[1] R. Dasari, J. Izatt, R. Richards-Kortum, R. Rava, and M. Feld, "An Overview of Activities at the Laser Biomedical Research Center," *IEEE Engineering in Medical and Biology Magazine*, December, pp. 14-20, 1989.

[2] M. Keijzer, R. Richards-Kortum, S. L. Jacques, and M. Feld, "Fluorescence spectroscopy of turbid media: Autofluorescence of the human aorta," *Applied Optics*, Vol. 28, No. 20, pp. 4286-4292, 1989.

[3] J. R. Lakowicz, H. Szmacinski, and M. L. Johnson, "Calcium Imaging Using Fluorescence Lifetimes and Long-Wavelength Probes," *J. of Fluorescence*, Vol. 2, pp. 47-61, 1992.

[4] C. L. Hutchinson, J. R. Lakowicz and E. M. Sevick-Muraca, "Fluorescence Lifetime-Based Sensing in Tissues: A Computational Study," *Biophysical Journal*, Vol. 68, pp. 1574-1582, 1995.

[5] M. S. Patterson, and B. W. Pogue, "A Mathematical Model for Time-Resolved, and Frequency-Domain Fluorescence in Biological Tissue," *Applied Optics*, Vol. 33, pp. 1965-1974, 1994.

[6] C. L. Hutchinson, T. L. Troy and E. M. Sevick-Muraca, "Fluorescence-lifetime spectroscopy and imaging in random media," *in Optical Tomography, Photon Migration, and Spectroscopy of tissue and Model media: Theory, Human Studies, and Instrumentation, B. Chance, and R. Alfano, eds, Proc. SPIE*, Vol. 2389, pp. 274-383, 1995.

[7] Y. Yao, "Forward and Inverse Studies for Optical Imaging," Ph. D. Dissertation, Polytechnic University, 1996.

[8] J. Chang, H. L. Graber, R. L. Barbour " Luminescence optical tomography of dense scattering media," *J. Opt. Soc. Am. A*, Vol. 14, no. 1 pp. 288-299, 1997.

[9] M. A. O'Leary, D. A. Boas, X. D. Li, B. Chance and A. G. Yodh, "Fluorescence Lifetime Imaging in Turbid Media," *Optics Letters*, Vol. 21, pp. 158-160, 1996.

[10] D. Y. Paithankar and E. M. Sevick-Muraca, "Fluorescence lifetime imaging with frequency-domain photon migration measurement," *OSA TOPs on Biomedical Optical Spectroscopy and Diagnostics, E. M. Sevick-Muraca and David Benaron, eds*, Vol. 3, pp. 184-194, 1996.

[11] J. Chang., R. L. Barbour, and H. L. Graber, and R. Aronson, "Fluorescence Optical Tomography," *in Experimental and Numerical Methods for Solving Ill-posed Inverse Problems: Medical and Nonmedical Applications, R. L. Barbour, M. J. Carvlin, and M. A. Fiddy, eds, Proc. SPIE*, Vol. 2570, pp. 59-72, 1995.

[12] Y. L. Pei, Y. Q. Yao, F. B. Lin, Y. Wang, and R. L. Barbour, "Optical Image Reconstruction for Turbid Media Using Finite Element Model," *Proc. Spectroscopy and Imaging in Scattering Media*, in *80th Anniversary OSA Annual Meeting & Exhibit*, Rochester, NY, October, 1996.

[13] W. W. Zhu, Y. Wang, R. L. Barbour, H. L. Graber and J. Chang, "Regularized Progressive Expansion Algorithm for Recovery of Scattering Media from Time-Resolved Data," in *OSA Proc. on Advances in Optical Imaging and Photon Migration*, R. R. Alfano, ed., pp. 211-216, 1994.

[14] R. L. Barbour, H. L. Graber, J. Chang, S. L. S. Barbour, P. C. Koo, and R. Aronson, "MRI-Guided Optical Tomography: Prospects and Computation for a New Imaging Method," *IEEE Comp. Sci. & Eng.*, Vol. 2, pp. 63-77, 1995.

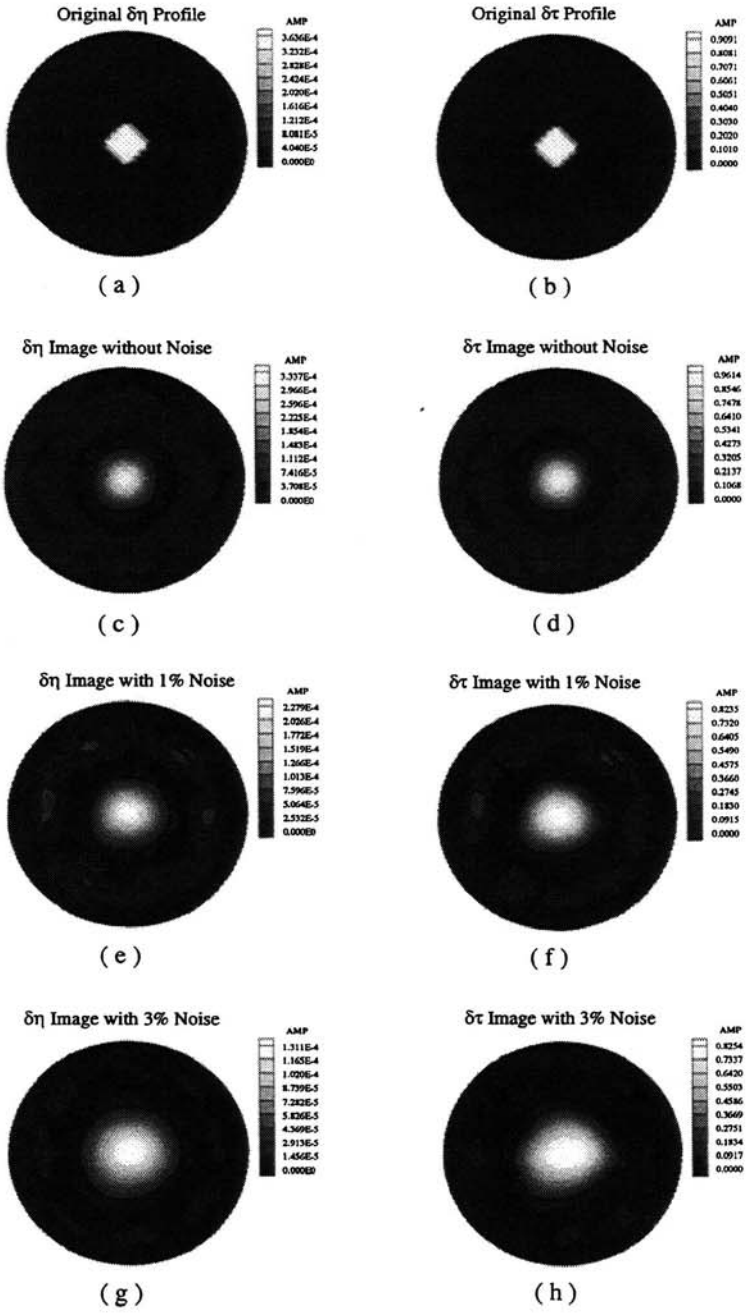

Figure 2: Reconstruction images of fluorescence yield $\delta\eta$ (left figure) and lifetime $\delta\tau$(nsec) (right figure) with and without added noise for Case I (simple medium) containing centered target. Perturbation = added fluorophore in target only; no fluorophore present in reference medium.

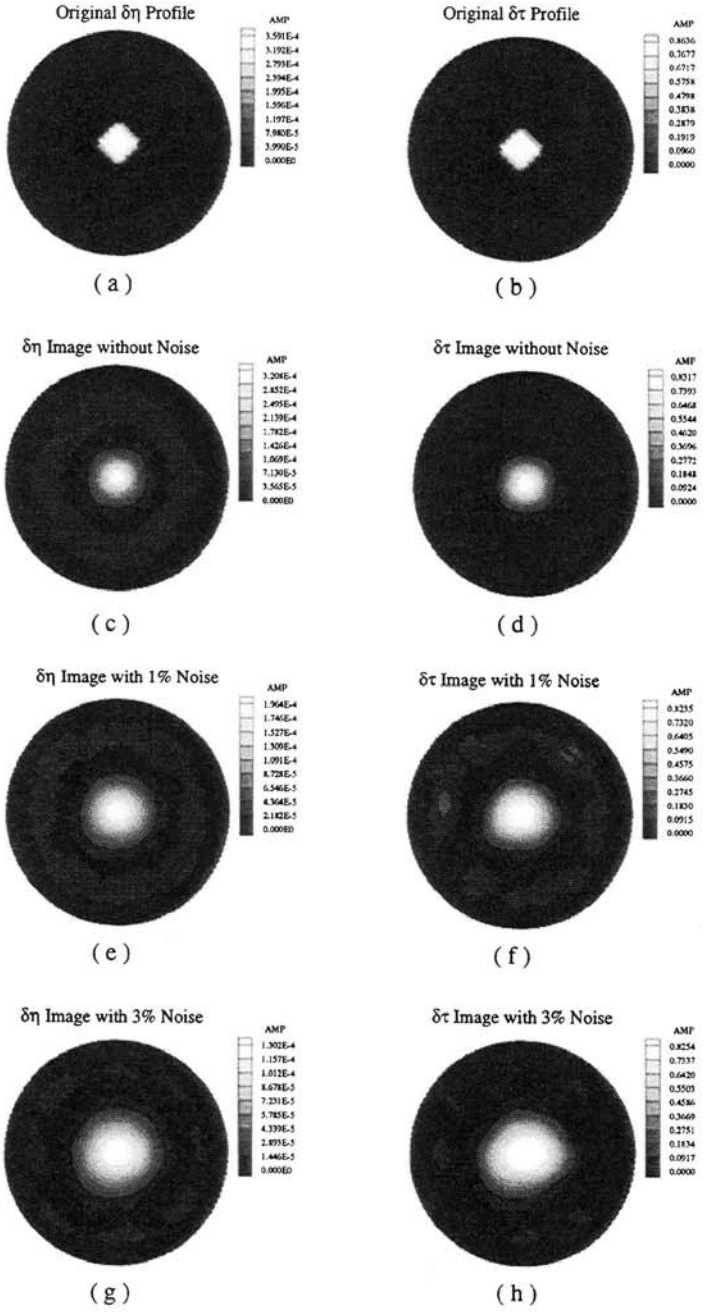

Figure 3: Reconstruction images of fluorescence yield $\delta\eta$ (left figure) and lifetime $\delta\tau$(nsec) (right figure) with and without added noise for Case II (simple medium) containing centered target. Perturbation = added fluorophore in target only; fluorophore present in background reference and target medium.

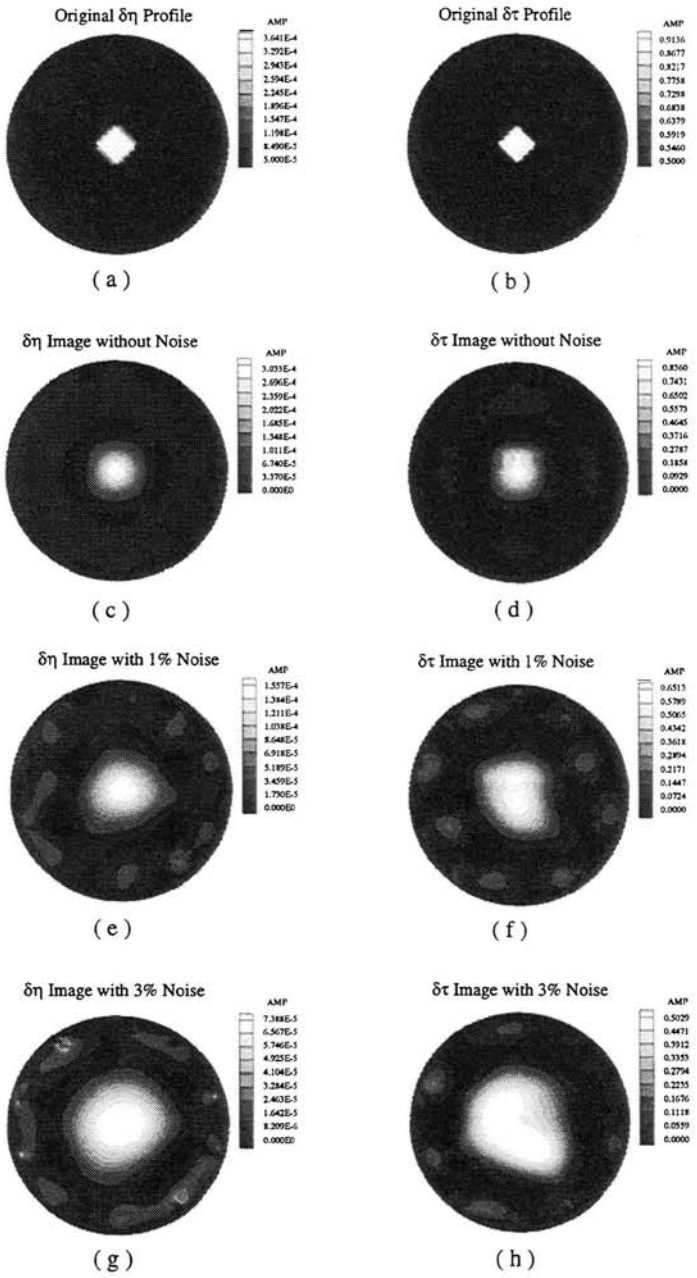

Figure 4: Reconstruction images of fluorescence yield $\delta\eta$ (left figure) and lifetime $\delta\tau$(nsec) (right figure) with and without added noise for Case III (simple medium) containing centered target. Perturbation = added fluorophore in target plus background; no fluorophore present in reference medium.

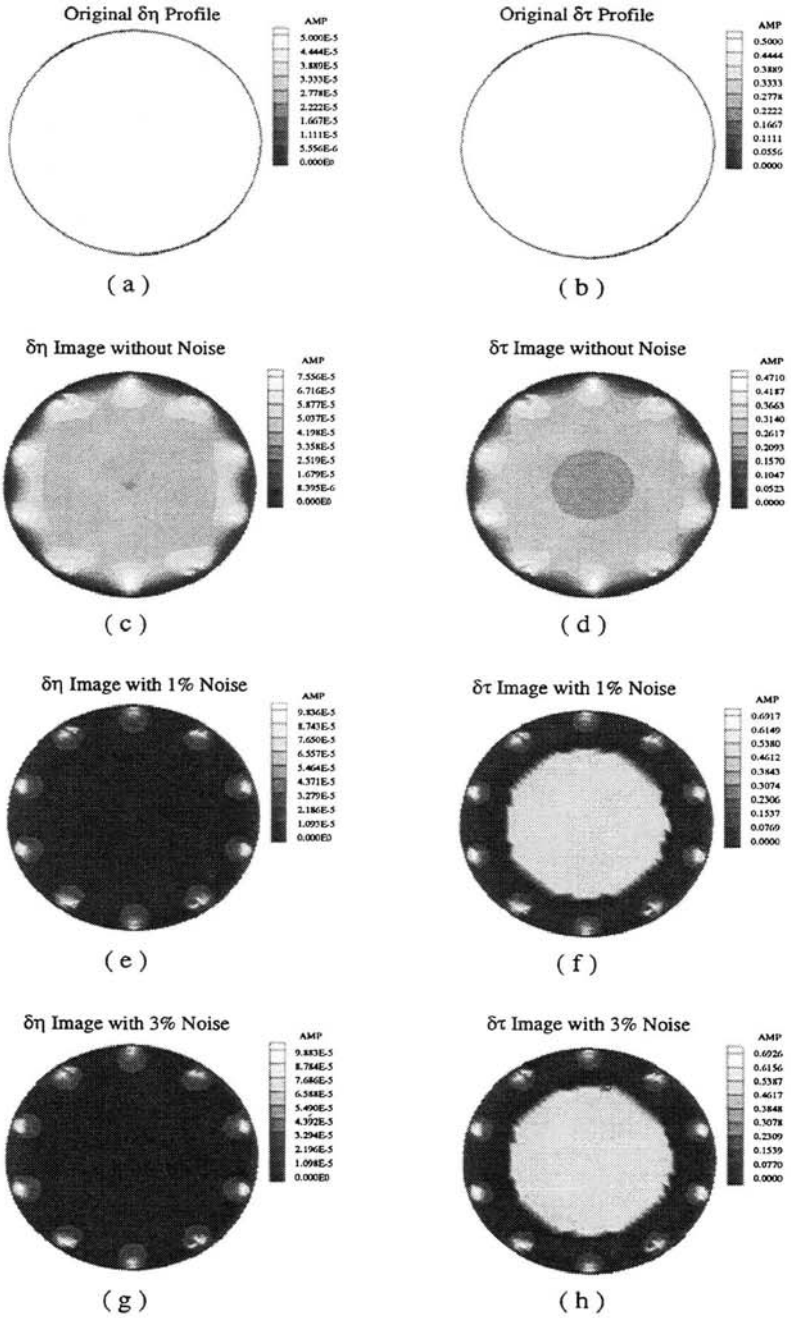

Figure 5: Reconstruction images of fluorescence yield $\delta\eta$ (left figure) and lifetime $\delta\tau$(nsec) (right figure) with and without added noise for Case IV (simple medium) without centered target. Perturbation = added fluorophore in background; no fluorophore present in reference medium.

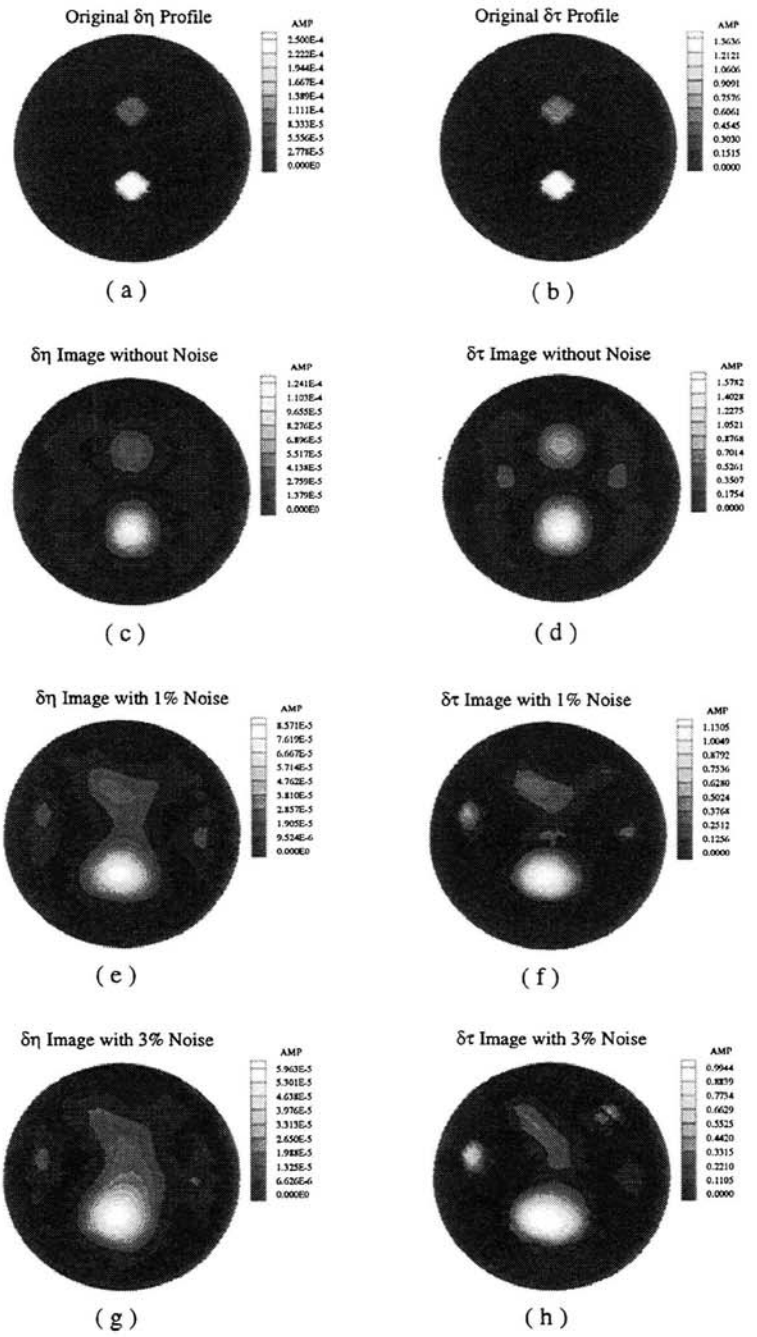

Figure 6: Reconstruction images of fluorescence yield $\delta\eta$ (left figure) and lifetime $\delta\tau$(nsec) (right figure) with and without added noise for Case V (MRI breast map) containing two separate targets. Perturbation = added fluorophore in target only; fluorophore present in background of reference and target medium.